Meteoritics & Planetary Science 37, 1765–1779 (2002)
Available online at http://www.uark.edu/meteor

Kgagodi Basin: The first impact structure recognized in Botswana

D. BRANDT[1], H. HOLMES[2], W. U. REIMOLD[1]*, B. K. PAYA[1], C. KOEBERL[3] AND P. J. HANCOX[1]

[1]Impact Cratering Research Group, School of Geosciences, University of the Witwatersrand, Private Bag 3, P.O. Wits 2050, Johannesburg, South Africa
[2]Department of Geological Survey, Private Bag 14, Lobatse, Botswana
[3]Institute of Geochemistry, University of Vienna, Althanstrasse 14, A-1090 Vienna, Austria
*Correspondence author's e-mail address: 065wur@cosmos.wits.ac.za

(Received 2002 April 4; accepted in revised form 2002 August 15)

Abstract–The 3.4 km wide, so-called Kgagodi Basin structure, which is centered at longitude 27°34.4' E and latitude 22°28.6' S in eastern Botswana, has been confirmed as a meteorite impact structure. This crater structure was first recognized through geophysical analysis; now, we confirm its impact origin by the recognition of shock metamorphosed material in samples from a drill core obtained close to the crater rim. The structure formed in Archean granitoid basement overlain and intruded by Karoo dolerite. The crater yielded a gravity model consistent with a simple bowl-shape crater form. The drill core extends to a depth of 274 m and comprises crater fill sediments to a depth of 158 m. Impact breccia was recovered only between 158 and 165 m depth, below which locally brecciated basement granitoids grade into fractured and eventually undeformed crystalline basement, from ~250 m depth. Shock metamorphic effects were only found in granitoid clasts in the narrow breccia zone. This breccia is classified as suevitic impact breccia due to the presence of melt and glass fragments, at a very small abundance. The shocked grains are exclusively derived from granitoid target material. Shock effects include multiple sets of planar deformation features in quartz and feldspar; diaplectic quartz, and partially and completely isotropized felsic minerals, and rare melt fragments were encountered. Abundances of some siderophile elements and especially, Ir, in suevitic breccia samples are significantly elevated compared to the contents in the target rocks, which provides evidence for the presence of a small meteoritic component.

Kgagodi is the first impact structure recognized in the region of the Kalahari Desert in southern Africa. Based on lithological and first palynological evidence, the age of the Kgagodi structure is tentatively assigned to the upper Cretaceous to early Tertiary interval. Thus, the crater fill has the potential to provide a long record of paleoclimatic conditions.

INTRODUCTION

In comparison to the impact cratering records of other continents, the record for the African continent (Koeberl, 1994; Master and Reimold, 2000) is poor. Only 18 impact structures have been confirmed, and large regions of Africa have remained entirely unexplored for impact craters. Reasons for this include inaccessibility of vast regions in central Africa due to dense rainforest cover and/or widespread political strife, and the fact that by far most geologists operating on the continent are still generally unaware of the importance of impact cratering. However, in recent years, several new impact structures have been discovered or proposed in Africa, mostly as a result of initial remote sensing studies (*e.g.*, Master and Reimold, 2000).

Botswana is a country of 582 000 km^2 area in southern Africa. About four-fifths of its terrane is covered by desert and semi-desert, represented by the substantial deposits of the Cretaceous to Holocene Kalahari Group (*e.g.*, Thomas and Shaw, 1990). Geophysical surveys of this country have, to date, not indicated the existence of any impact structures in Botswana, but the size of this area (*e.g.*, in comparison to parts of Scandinavia and Eurasia) suggests that several such structures ought to exist here.

A sediment-filled, slightly elliptical, basin-like structure (the so-called Kgagodi Basin) was first recognised in 1997/1998 during a water-drilling project in southeastern Botswana (Fig. 1a). It is located ~7 km south of Kgagodi village (Fig. 1b), along the old Kgagodi-Maunatlala road and northeast of the Tswapong Hills. The basin structure is centered at 22°29' S and 27°35' E. The ~3.4 km diameter structure had previously been mapped from aerial photography and satellite imagery (Thomas, 1971; Paya *et al.*, 1999), but had never been investigated. Only in the course of a regional hydrological project did it attract further attention. Finally, in 1997, the structure was drilled by the

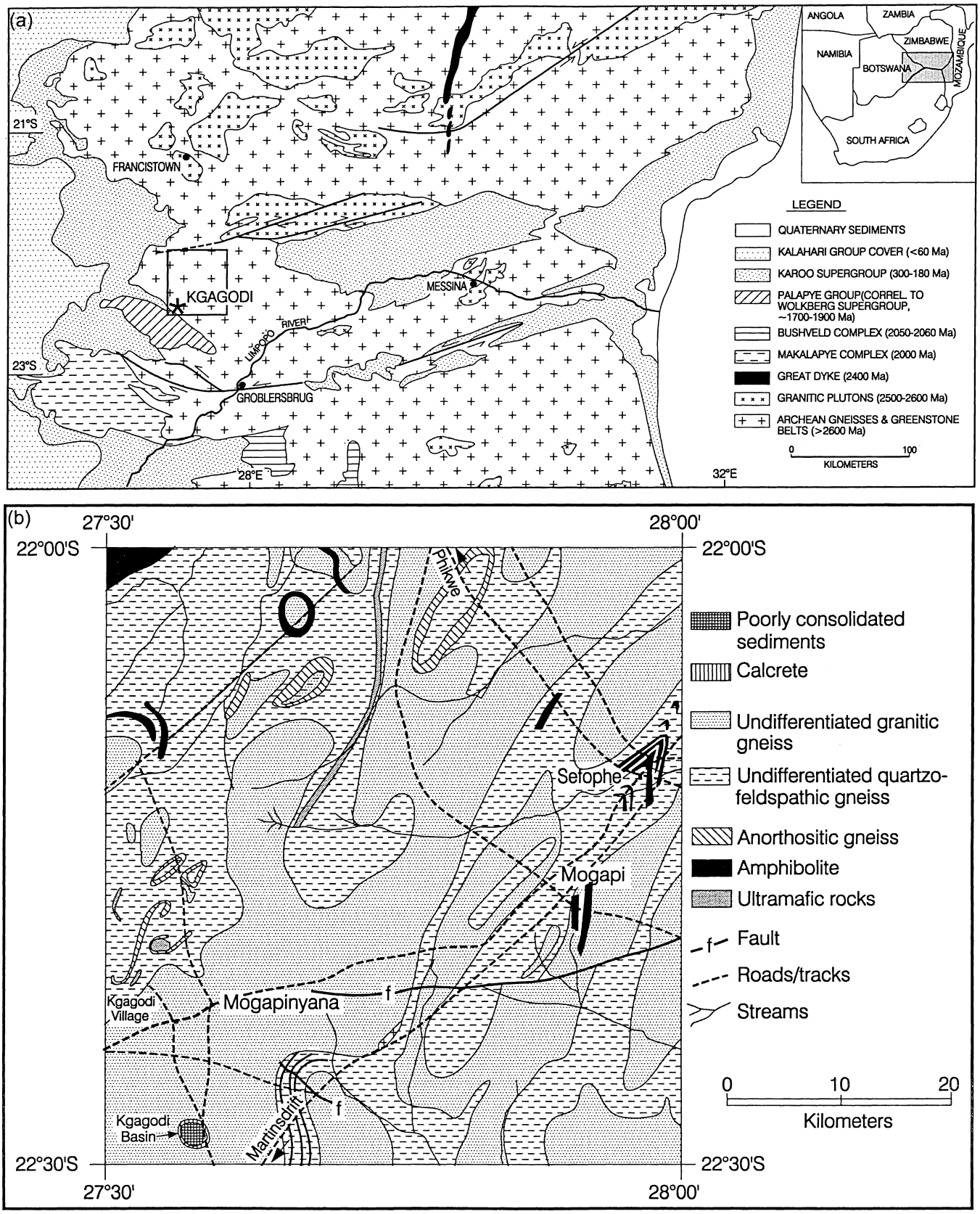

FIG. 1. (a) Regional geological map of the area surrounding the Kgagodi Basin; (b) detailed geological map of the Kgagodi Basin and environs.

Geological Survey of Botswana to a depth of 274 m, as it was thought to represent the intersection of two fault lines and, thus, considered a prospective hydrological target. On the surface, the structure (Fig. 2) only shows very rare and small outcrops, basically limited to some disseminated calcrete exposures, mostly along the crater rim. The remainder of this area is covered by alluvium that is overgrown by grass and rather dense acacia thorn-brush. Locally, subsistence farming takes place in areas covered with thick topsoil.

Initial investigations provided some results that led to the interpretation of Kgagodi as a possible impact structure (Paya *et al.*, 1999). However, at that time no definite evidence for impact had been found (*e.g.*, in the form of shock metamorphic deformation effects in rocks from the interior of this structure).

Here, we provide a detailed account of the geological setting of the Kgagodi structure, comprehensive geophysical data, and a report on petrographical and geochemical data obtained on drill core samples that provide evidence for an impact origin of this structure. Some early results were presented by Reimold *et al.* (2000).

REGIONAL GEOLOGY

The so-called Kgagodi Basin structure is situated in the Central Zone of the Limpopo Mobile Belt (Watkeys, 1983; McCourt and Vearncombe, 1992). The topographic expression of this structure (which ideally should not have been given the name "basin") only involves a slightly (±1 m) raised rim feature characterized by a series of discontinuous calcrete exposures. The area of the structure is essentially flat. The region around the structure (Fig. 1b) comprises limited exposures of Archean high-grade gneisses, amphibolites, ultramafics, granitic gneisses and migmatites, all of which belong to the crystalline basement complex. The Archean lithologies are overlain by metasedimentary rocks of the Palapye group, considered part of the Waterberg Supergroup of approximately 1.7–1.9 Ga age (Watkeys, 1983; McCourt and Vearncombe, 1992). Still younger formations include extensive Karoo (300–180 Ma) sediments, as well as some Karoo dolerite intrusions in the form of dikes and sills.

In the closer environs of the Kgagodi structure, granitic exposures and a sizable occurrence of Karoo dolerite occur in several hills ~1 km south of the basin. No macro-deformation possibly related to the formation of the crater structure could be observed at this locality. Sporadic amphibolite exposures and loose boulders occur along the southern edge of the basin. The remainder of the area, as indicated by the aerial photograph (Fig. 2), is generally flat to slightly undulating, with little or no outcrop, besides the isolated, surficial calcrete deposits along the edge of the basin (the crater rim trace in Fig. 2 coincides with their positions). The streams at and near Kgagodi village form part of the Tshokana River drainage system, which is, in turn, part of the Limpopo drainage system. Aerial photography does not indicate any influence on the local drainage system due to the existence of the basin structure.

GEOPHYSICAL INVESTIGATIONS

Survey Design and Methodology

Gravity measurements were first obtained in 1998 to outline the extent of the structure and to investigate the possible presence of fault structures in this area. Gravity measurements were obtained along two profiles oriented north–south and east–west and passing through the center of the feature. More recently, measurements along four additional profiles (two parallel to each of the earlier orientations and ~1.5 km from the center of the structure) of limited extent (Fig. 2) were obtained. The primary, central, north–south and east–west lines extended ~3 km beyond the apparent limit of the structure (as seen on the aerial photograph; Fig. 2), representing an attempt to obtain regional background values. The four other, secondary lines were a little more than half the length of, and parallel to, the primary lines. Magnetic data were also collected along each of these profiles. Leveling and a differential global positioning system (GPS) were used for elevation control with readings taken at 50 m intervals. A site at the approximate center of the structure was chosen as base station.

Data Acquisition and Processing

The gravity readings were merged with the elevation control data and reduced to Bouguer anomaly values using the Geosoft GRAVRED software (GRAV2DC version 1.59, unpublished program, G. R. J. Cooper, Dept. of Geophysics, Univ. of the Witwatersrand, Johannesburg, South Africa). Data were corrected for the following effects: instrument drift, tides, latitude, free-air and Bouguer density corrections. Magnetic values were corrected for diurnal variations.

Data Interpretation and Results

Only the results of the primary profiles are presented here, as the main features of the survey are clearly exhibited in these profiles. The other profiles show similar features, and their presentation would constitute repetition.

Gravity–The results of the gravity survey are shown in Fig. 3a,b. Forward modeling of the data indicated that the maximum depth of the central part of the basin is ~900 m and that the modeled diameter is similar to that defined by the subcircular array of calcrete exposures along the margin of the structure at 3–4 km diameter. Contrasted against a Bouguer density of 2.67 g/cm^3, the sediment infill shows a density contrast of about –0.45 g/cm^3, whereas the basement shows a density contrast of 0.145 g/cm^3. As shown in Fig. 3a,b, the gravity results clearly delineate the density contrast between the dense basement and less dense sedimentary infill, with a

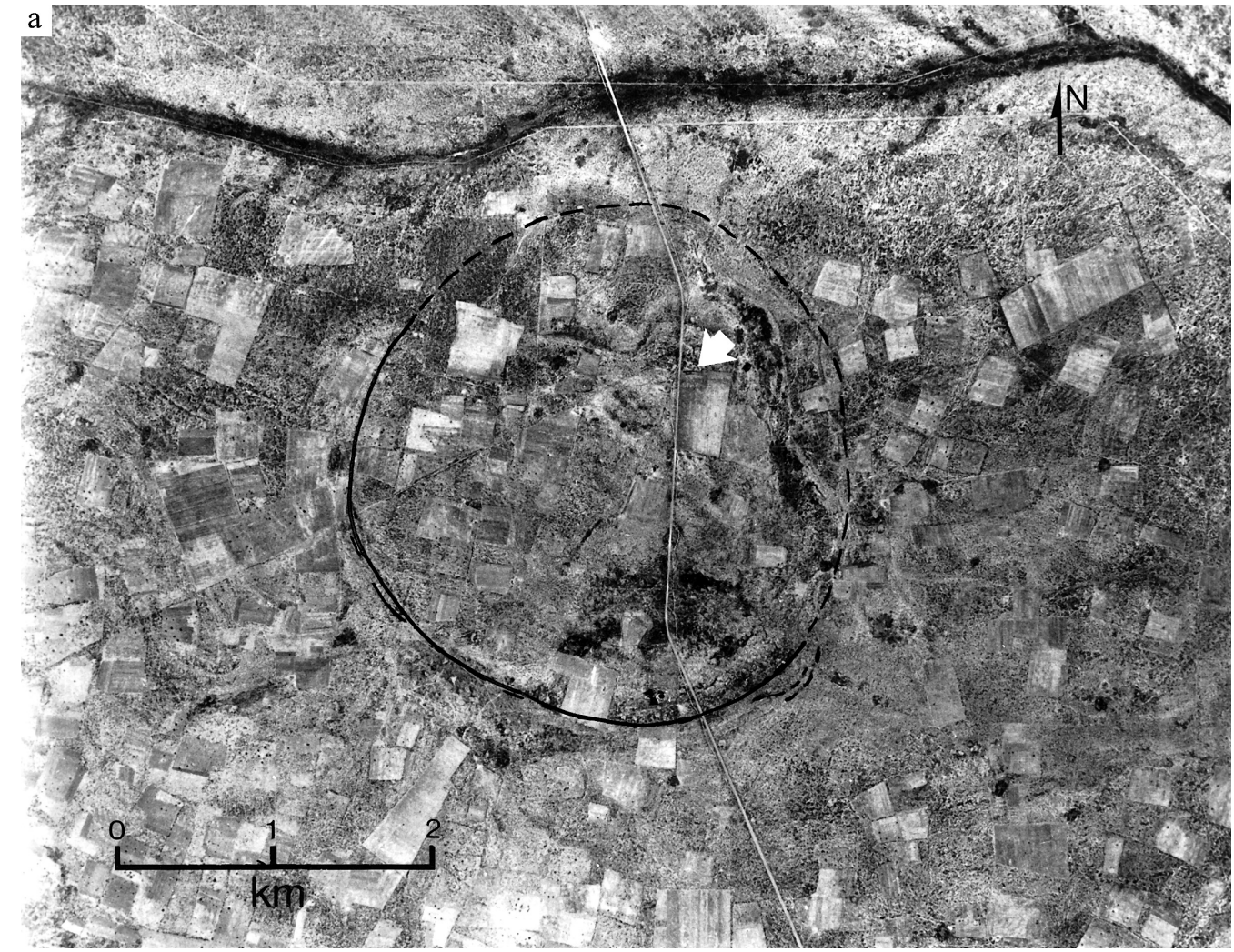

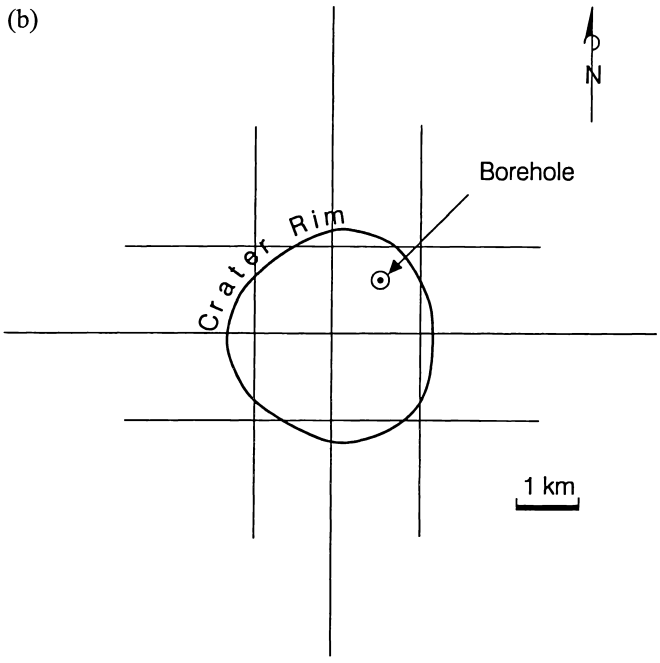

FIG. 2. (a) Aerial photograph of the Kgagodi Basin showing the approximate position of the calcretized rim feature. The arrow indicates the site of the borehole. (b) The north–south and east–west lines correspond to the magnetic and gravity profiles measured first across the crater. The shorter, parallel, north–south lines were measured during 2000. The long profiles extend beyond the limits of the area shown.

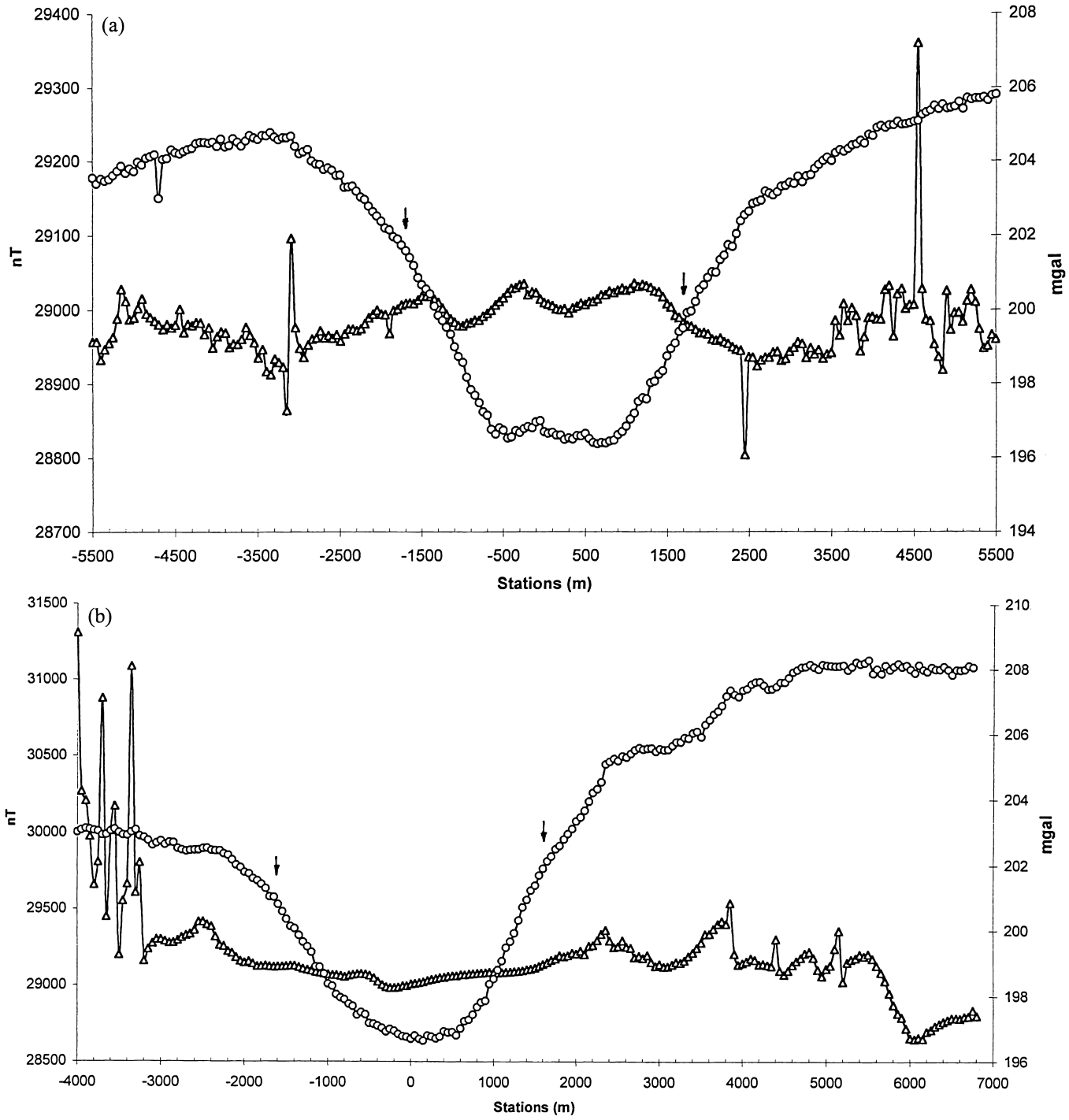

FIG. 3. (a) South–north and (b) east–west Bouguer gravity and magnetic profiles across the Kgagodi Basin. Open triangles represent magnetic data and open circles are Bouguer gravity values. Arrows indicate the position of the crater rim—outside of which the "regional trend" was measured.

large negative anomaly of up to 10 mGals. The slightly elliptical geometry of the structure that is discernable from satellite imagery and aerial photography (Fig. 2) is also confirmed by the trace of the inflection points on the gravity profiles. As indicated by the east–west profile (Fig. 3b) and, to a lesser degree, in the north–south profile, there appears to be a fairly strong regional trend. The exact regional trend is not entirely discernable from the outer parts of the profiles, as they do not extend far enough beyond the margins of the structure. Another possibility of the great variation in the regional values, such as

that seen in the east–west profile (Fig. 3b), is that the structure coincides with a fault zone, which could greatly change the regional values from one side of the structure to the other.

Magnetics–The gravity low (Fig. 3a) is coincident with the inflection points between the noisy magnetic basement outside of the structure and the smooth sediment signature over the interior of the structure. The noisy high-frequency magnetic signature over the basement indicates shallow bodies of various magnetic susceptibilities, as would be expected for a complex geological terrane composed of gneissic and migmatitic rocks that are intruded by mafic dikes. The more gently undulating signature over the sediment-filled structure, particularly along the north–south profile (Fig. 3b), is distinctly different from the magnetic expression of the immediate environs of the structure, where the magnetic field has been "smoothed" by the sedimentary infill of the crater. The sediments are magnetically more homogeneous than the surrounding basement and hide the expression of the underlying noisy basement.

After completion of the geophysical analysis, it became clear that the drill core through the entire structure had been obtained relatively close to (<400 m inside of) the crater rim in the northeastern corner of the structure (see Fig. 2). This position close to the edge of the crater infers that the drill core only sampled a rather limited section through the crater fill and floor.

DRILL CORE STRATIGRAPHY

A number of shallow percussion and solid drill cores had already been obtained prior to 1998. Based on chips and core bits still lying close to the drilling site inside of the crater structure, most material recovered at that time was calcrete. The remainder of these cores still found on surface was strongly weathered or even disintegrated when examined by our group in 2000. In 1997, the Geological Survey of Botswana obtained a drill core through the complete basin-fill and extending into the underlying basement. A schematic log for this drill core is shown in Fig. 4. The upper 60 m of the core comprise predominantly unconsolidated sands with varying amounts of carbonate material in the form of calcrete layers and marl. From ~60 to 158 m, the predominant basin fill is marl or limestone. This section overlies ~5 m of a coarse, poorly-consolidated breccia (Fig. 5a), which is described in some detail below. Below this formation, fractured granitoid basement comprising a wide range of mineralogically diverse lithologies, including leucogranite, granodiorite, diorite, and minor amphibolite, was transected (Fig. 5b,c), which eventually grades, with depth, into less fractured and, finally, undeformed basement, which was encountered at ~254 m depth. At 240 m depth, a 1 cm wide crosscutting band of breccia composed of abundant fine-grained, granitoid-derived clasts in an extensively weathered matrix was encountered, which could represent a possible injection into, or local formation of a melt breccia in the crater floor. The true nature of this material can, however, no longer be ascertained due to extensive alteration of the matrix.

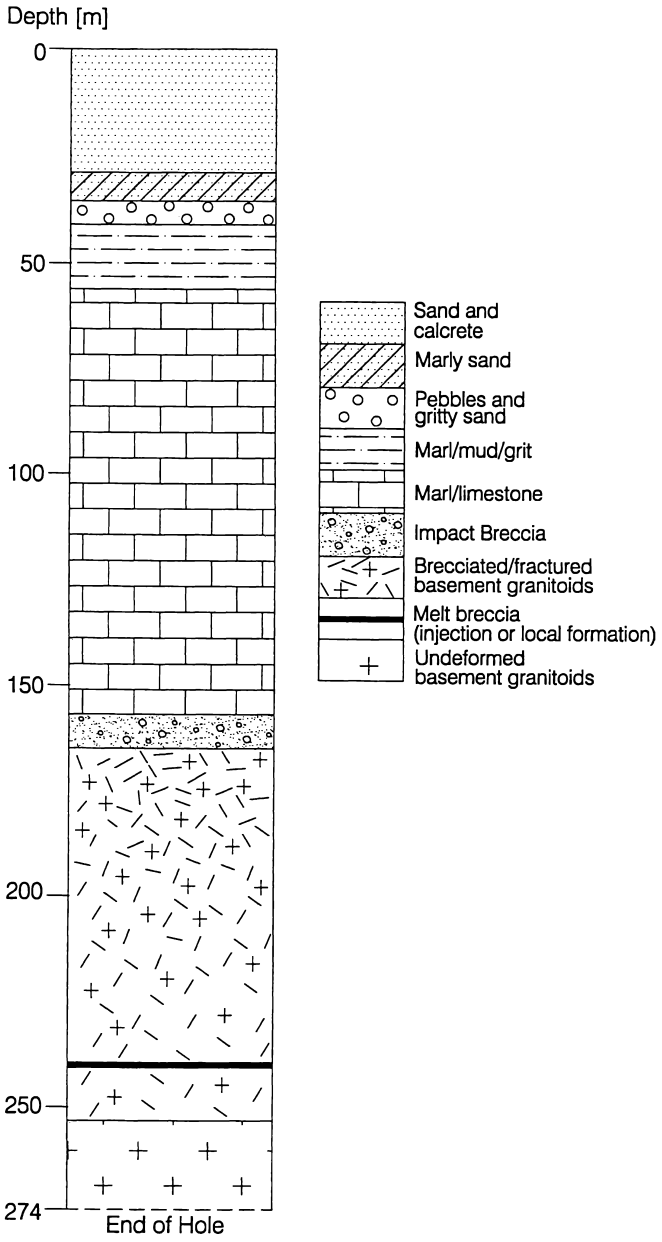

FIG. 4. Simplified schematic log for the drillcore obtained in the structure (see arrow in Fig. 2).

The sedimentary portion of this drill core will be discussed in detail in a separate paper (Hancox *et al.*, unpubl. data), focusing on the post-basin-formational paleoenvironmental record. However, for completion, several chemical analyses obtained on sediment samples will be reported here, in comparison to analytical results obtained for other drill core lithologies.

PETROGRAPHIC RESULTS

Several samples from each of the lithologies in the borehole were sampled and studied petrographically. The breccia

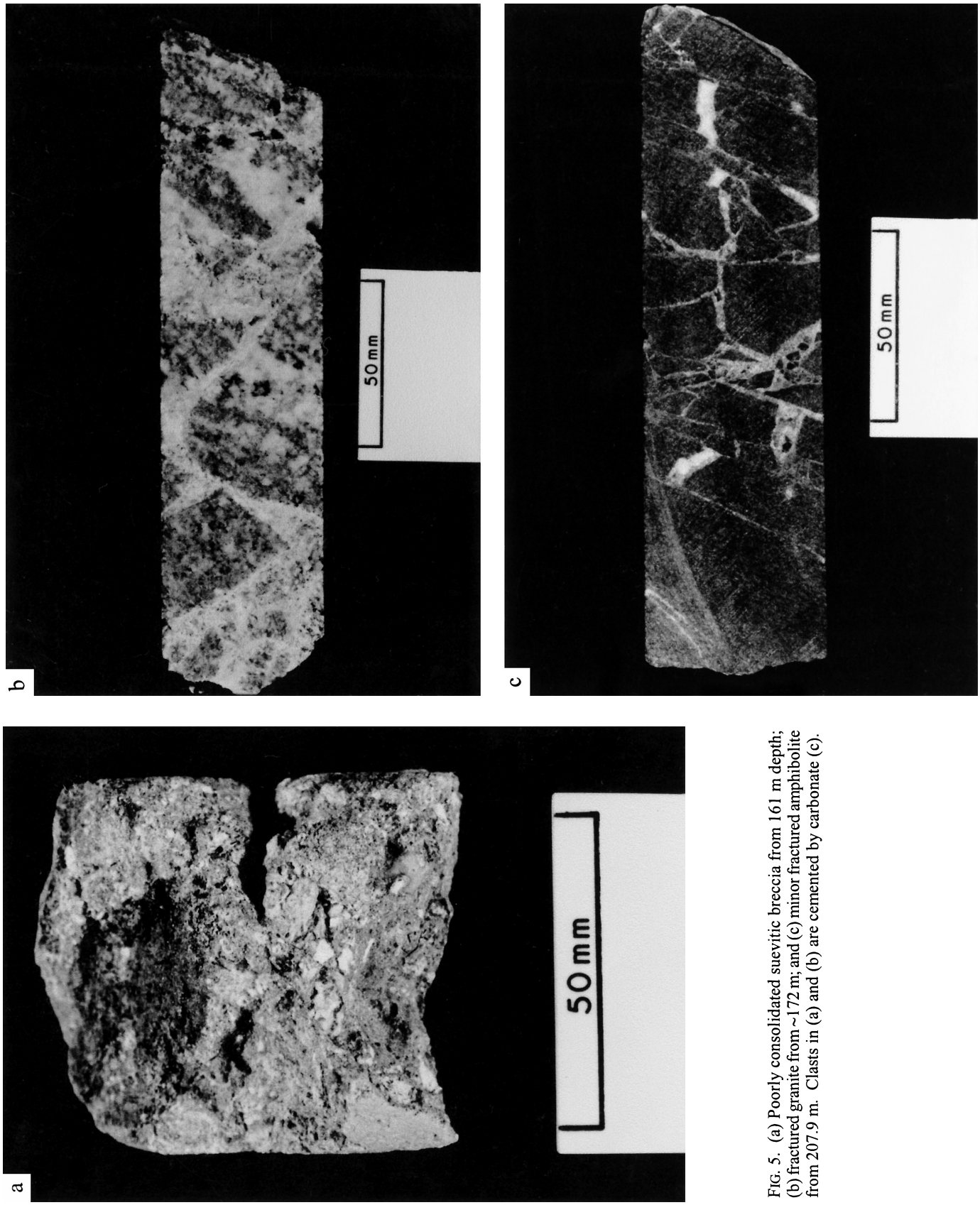

FIG. 5. (a) Poorly consolidated suevitic breccia from 161 m depth; (b) fractured granite from ~172 m; and (c) minor fractured amphibolite from 207.9 m. Clasts in (a) and (b) are cemented by carbonate (c).

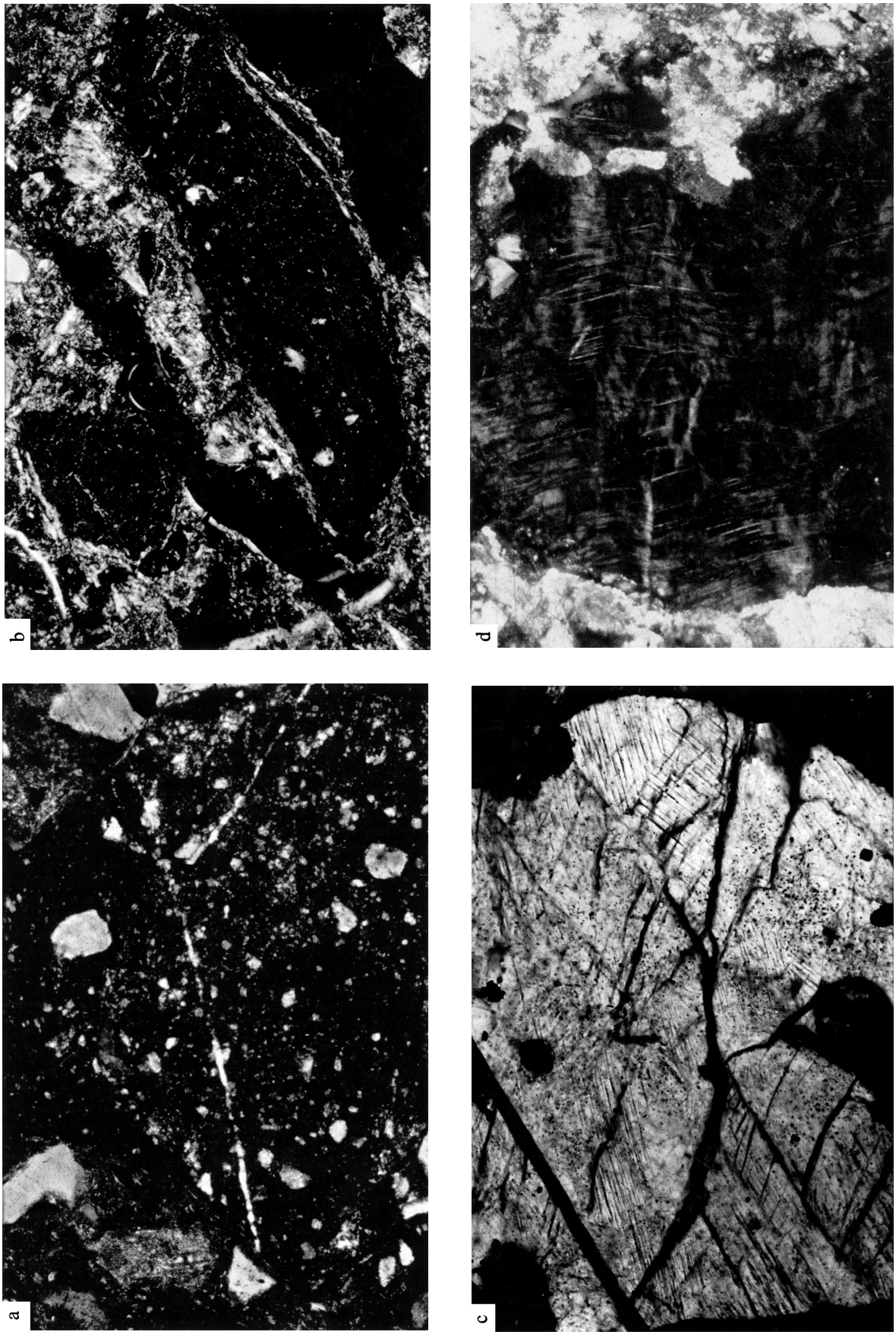

FIG. 6. (a) Impact melt fragments within suevitic impact breccia in sample 7G from 159.3 m (crossed polarized light: field of view = 1.75 mm). (b) Shock-melted portion of a large granitic fragment, several centimeters across, in a suevitic impact breccia (sample 7F; 164.7 m depth). This granitic clast also displays many grains of alkali feldspar and quartz grains with multiple sets of planar deformation features (PDFs), not shown here (plane polarized light: field of view = 2.2 mm). (c) PDFs in quartz in a clast in suevitic impact breccia (sample 7H) from 160.8 m (crossed polarized light: field of view = 0.9 mm). (d) Kinked and twinned alkali feldspar grain in sample 7E from 164 m depth (crossed polarized light: field of view = 1.1 mm).

intersected in the depth interval of 158–165 m contained little but definite evidence of shock metamorphism, as well as several partially melted clasts, and even melt fragments and devitrified glass. On the basis of this combined evidence, detailed below, it is classified as suevite. Figure 6a,b shows typical melt blebs in a clast and devitrified glass, respectively. Impact melt is generally aphanitic to cryptocrystalline, whereby finest grained crystallization products are thought to be the result of both incipient crystallization (devitrification) and alteration. The melt rock fragments contain abundant, tiny clasts of mostly granitoid-derived minerals (quartz, feldspar minerals, and some oxidic remnants presumably of biotite and/or amphibole). It can, however, not be excluded that some quartz is derived from a sedimentary component, as a few centimeter-sized clasts of sedimentary precursor rocks (sandstone and arkose) were noted macroscopically. As no such material could be unambiguously identified at the microscopic scale, it is thought that such a sedimentary component did not significantly contribute to the breccia formation in this borehole. This conclusion is also consistent with the chemical analyses obtained for suevitic breccias from Kgagodi, which are characterized by intermediate SiO_2 contents (compare Table 1). Locally, impact melt fragments contain fractures, which are often filled with carbonate or phyllosilicates. As exhibited by Fig. 6b, some melt fragments/blebs are heterogeneously structured with alternating schlieren of clast-poor and clast-rich melt. Flow structures in glass and clast alignment in clast-rich schlieren do occur but are not particularly prominent.

Numerous impact-diagnostic, multiple sets of planar deformation features (PDFs) were observed in quartz and feldspar grains (Fig. 6c,d) from clastic and melt portions of the suevitic breccia. Our observations do not allow to suggest that different shock degrees are indicated by the shock metamorphic effects observed in these two components of the breccia. The very poorly sorted clast population of suevitic breccia is dominated by granitic lithic and obviously granitoid-derived mineral clasts, besides a small but prominent component of gabbroic clasts and very little sediment-derived material. Clast sizes are mostly in the range between 1 cm and <1 mm, but rare larger fragments were also encountered. Sizes of melt fragments range from ~0.4 mm to a maximum of 2.5 cm. Gabbro clasts are generally texturally similar to gabbro sample #43 collected outside of the crater rim. Because of the characteristic texture comprising blade-shaped plagioclase and oikocrysts of pyroxene, these gabbro clasts and sample #43 are thought to represent Karoo dolerite intrusions. Karoo intrusions of generally 180 Ma age occur widespread in most regions of southern Africa (*e.g.*, Hargraves *et al.*, 1997 and references therein). This observation constrains the upper age limit for the impact event at <180 Ma.

Monomict fragmental breccias of basement granitoids and fractured basement rocks, as well as several specimens of suevitic breccia from the drill core, have been subject to calcite impregnation or calcite infilling in fractures or open spaces

TABLE 1. Chemical data for drill core samples (target rock and breccias) analyzed by XRF and INAA.

Sample	2	2A	3	4A	5A	6A	7C	7E	7F	7G	7J	7K	14A	14B	14E	14F	16	20	41	42	43
	schist	granitoid	basement granitoid	basement granitoid	basement granitoid	basement granitoid	suevitic breccia	suevitic breccia	breccia	suevitic breccia	granite gneiss	breccia	breccia	brecciated limestone	basement clast	granite clast	limestone	granite clast	basement granitoid	granite	gabbro
Depth (m)	252.5	250	249.5	240.8	240	213	195.2	164	164.7	159.3	157.8	157	156.6	152.8	146	141.5	125.6	95.3	0	0	0
SiO_2	45.7	58.6	67.39	55.9	54.27	65.38	62.6	53.41	64.63	55	44.16	51.85	65.64	29.08	53.48	62.84	56.05	70.68	72.03	67.55	53.61
TiO_2	1.74	0.39	0.06	1.17	1.4	0.32	0.62	0.38	0.4	0.52	0.46	0.98	0.49	0.3	0.5	0.45	0.57	0.37	0.3	0.52	0.76
Al_2O_3	13.65	12.96	9.82	12.72	13.38	12.72	11.54	9.89	11.8	16.18	9.95	16.4	13.79	6.56	10.99	13.47	11.9	14.48	14.33	14.94	14.9
Fe_2O_3	13.93	2.6	0.58	8.36	8.18	1.92	3.85	2.77	2.85	6.31	3.54	7.79	3.24	2.82	3.41	2.75	3.9	2.79	2.48	2.91	9.95
MnO	0.29	0.11	0.07	0.05	0.05	0.06	0.09	0.18	0.05	0.09	0.08	0.1	0.04	0.12	0.05	0.03	0.04	0.02	0.02	0.04	0.18
MgO	5.76	1.76	0.53	3.69	4.14	1.67	2.21	2.29	2.24	8.45	4.21	7.32	2.48	6.35	3.31	3.2	5.34	1.13	0.53	0.64	6.65
CaO	10.3	10.77	9.39	4.12	3.03	5.34	7.86	12.5	3.98	1.08	16.02	5.31	3.1	22.95	9.23	5.55	5.3	2.78	2.19	1.93	10.02
Na_2O	3.17	2.4	2.75	1.61	0.9	4.62	2.54	1.79	2.12	4.36	1.18	2.49	2.34	0.45	0.7	2.88	1.65	4.57	3.68	4.45	2.05
K_2O	0.94	1.32	2.02	1.14	1.39	2.37	1.29	1.6	2.02	1.92	1.42	1.65	2.02	0.82	2.14	2.13	1.72	2.21	3.25	5.16	1.06
P_2O_5	0.17	0.13	0.03	0.23	0.49	0.09	0.3	0.1	0.11	0.18	0.16	0.72	0.12	0.14	0.14	0.13	0.12	0.11	0.08	0.16	0.1
LOI	4.68	9.37	7.54	10.39	13.11	5.76	6.94	15.27	10.24	6.18	18.22	5.95	7.14	30.02	16.1	7.04	13.71	1.01	1.35	0.52	1.01
Total	100.33	100.41	100.18	99.38	100.34	100.25	99.84	100.18	100.44	100.27	99.4	100.56	100.4	99.61	100.05	100.47	100.3	100.15	100.24	98.82	100.29
Sc	38.2	2.66	0.97	9.59	10.9	0.91	4.07	4.71	4.13	5.57	5.03	20.1	5.21	4.57	5.67	4.01	6.88	3.66	2.28	3.73	37.6
V	369	45	<15	111	77	21	49	49	38	96	53	108	40	40	33	40	57	33	23	20	227
Cr	110	24.5	10.7	79.5	83.9	17.4	22.6	209	162	86.9	119	476	100	201	87.1	49.2	208	23.3	15.4	33.7	139
Co	44.4	8.82	2.5	24.5	22.7	5.27	14.9	14.2	10.1	18.8	11.9	24.8	9.21	13.1	11.5	8.68	14.5	6.95	5.37	7.79	47.3
Ni	69	18	7	61	58	14	25	66	54	60	65	138	40	52	48	27	78	10	10	18	90

TABLE 1. *Continued.*

Sample	2 schist	2A granitoid	3 basement granitoid	4A basement granitoid	5A basement granitoid	6A basement granitoid	7C suevitic breccia	7E suevitic breccia	7F suevitic breccia	7G suevitic breccia	7J granite gneiss	7K suevitic breccia	14A breccia	14B brecciated limestone	14E basement clast	14F granite clast	16 limestone	20 granite clast	41 basement granitoid	42 granite	43 gabbro
Depth (m)	252.5	250	249.5	240.8	240	213	195.2	164	164.7	159.3	157.8	157	156.6	152.8	146	141.5	125.6	95.3	0	0	0
Cu	72	<2	<2	9	24	<2	<2	<2	<2	<2	7	28	<2	<2	4	<2	<2	<2	<2	<2	61
Zn	149	49	17	118	141	34	76	47	40	162	45	139	94	53	74	62	79	57	42	55	81
As	0.35	0.25	0.35	0.4	0.46	0.3	0.2	0.3	0.95	0.36	0.25	0.3	0.2	0.3	0.42	1.12	0.66	0.55	0.51	1.35	3.03
Se	0.27	0.06	0.09	0.07	0.18	0.14	0.25	0.16	0.14	0.04	0.09	0.19	0.08	0.17	0.08	0.11	0.08	0.11	0.05	0.36	0.11
Br	2.1	0.65	0.95	1.2	1.1	1.5	1.2	0.9	1.1	0.75	0.85	0.85	0.95	0.83	0.65	0.32	0.59	1.3	0.72	2.6	1.2
Rb	35.2	47.3	110	77.1	109	90.2	68.9	57.5	60.7	54.9	57.6	70.6	81.4	54.9	115	96.2	70.5	106	117	118	48.1
Sr	188	345	77	203	153	178	289	112	92	60	250	382	185	390	135	285	238	167	159	810	148
Y	26	12	10	36	35	19	18	25	18	17	17	34	14	18	18	12	18	11	10	22	25
Zr	120	125	9	245	420	175	199	125	135	191	155	235	188	120	190	183	205	215	155	310	100
Nb	16	6	6	17	29	8	13	6	7	9	9	11	11	7	12	9	10	12	10	13	8
Sb	0.02	0.03	0.21	0.16	0.11	0.09	0.05	0.14	0.17	0.11	0.12	0.18	0.27	0.15	0.35	0.18	0.11	0.06	0.05	0.19	0.29
Cs	0.17	0.7	2.34	1.25	2.15	0.79	1.61	1.22	1.31	0.16	1.14	0.48	1.55	0.95	1.52	0.93	0.87	0.94	0.54	0.21	2.35
Ba	175	480	85	365	390	590	555	475	423	480	430	570	528	250	550	620	430	687	820	2250	280
La	21.2	27.2	12.4	47.5	141	66.7	53.1	30.4	21.4	21.5	32.7	57.3	29.7	37.4	51.7	39.1	45.1	34.4	33.7	109	16.6
Ce	41.8	44.7	12.7	99.3	244	100	84.9	43.5	33.8	41.3	62.4	131	51.7	64.3	76.7	61.1	76.2	54.8	54.1	188	33.9
Nd	22.4	18.5	7.79	51.8	102	41.3	35.5	20.3	16.4	19.5	29.1	78.7	24.1	30.5	34.2	28.9	33.8	22.7	20.9	88.9	15.9
Sm	5.01	2.48	1.35	12.1	15.2	6.05	5.51	3.85	3.05	3.17	4.51	14.3	3.57	7.29	5.65	4.72	6.35	3.42	3.02	12.7	3.81
Eu	1.41	0.85	0.41	2.11	1.89	1.06	1.14	1.14	0.85	0.95	0.91	2.79	0.89	0.88	0.94	0.88	1.02	0.82	0.71	2.62	1.01
Gd	4.36	2.11	1.12	12.6	13.1	4.6	4.24	4.3	2.63	3.1	3.95	11.1	3.09	4.01	3.5	3.05	4.89	2.8	2.2	12.2	3.52
Tb	0.75	0.26	0.17	1.55	1.35	0.52	0.49	0.6	0.45	0.44	0.49	1.31	0.42	0.51	0.5	0.37	0.56	0.33	0.24	0.98	0.67
Tm	0.39	0.11	0.052	0.58	0.46	0.21	0.2	0.31	0.27	0.26	0.21	0.55	0.18	0.24	0.22	0.19	0.26	0.14	0.09	0.38	0.43
Yb	2.52	0.56	0.32	3.26	2.51	1.19	1.05	1.91	1.92	1.86	1.04	3.01	0.95	1.31	1.18	0.93	1.41	0.65	0.45	1.49	2.76
Lu	0.35	0.085	0.045	0.45	0.39	0.15	0.15	0.29	0.23	0.36	0.14	0.39	0.15	0.19	0.19	0.13	0.22	0.1	0.066	0.18	0.36
Hf	3.38	2.64	0.14	5.09	9.53	4.18	4.49	2.57	3.13	5.06	3.38	5.88	5.02	2.24	4.72	4.48	4.19	5.88	4.07	7.67	2.92
Ta	0.77	0.095	0.67	1.17	2.36	0.34	0.81	0.28	0.26	0.36	0.37	0.39	0.45	0.32	0.65	0.41	0.46	0.73	0.29	0.92	0.32
Ir (ppb)	<1.1	<0.9	<0.6	<0.7	<2	<0.5	<0.7	<0.5	<1	0.6	<1	<1	0.18	0.52	<0.7	<1	0.7	<0.5	<0.5	<0.3	<0.3
Au (ppb)	0.6	0.2	0.2	0.4	0.9	1.3	0.4	0.4	0.3	0.3	0.2	0.8	0.2	1.1	1.4	1.2	0.9	0.3	0.5	0.5	0.5
Th	1.57	1.71	4.43	41.2	47.3	25.8	13.4	4.86	4.49	10.4	11.8	2.43	14.4	6.92	15.7	13.1	11.1	22.1	17.9	67.9	4.75
U	0.48	0.41	0.29	3.19	7.53	2.19	2.18	2.47	0.93	1.33	3.46	1.28	1.46	20.5	4.31	4.82	8.62	1.26	1.07	3.91	0.75
K/U	16319	26829	58046	2978	1538	9018	4931	5398	18100	12030	3420	10742	11530	333	4138	3683	1663	14616	25312	10997	11778
Zr/Hf	35.50	47.35	64.29	48.13	44.07	41.87	44.32	48.64	43.13	37.75	45.86	39.97	37.45	53.57	40.25	40.85	48.93	36.56	38.08	40.42	34.25
La/Th	13.50	15.91	2.80	1.15	2.98	2.59	3.96	6.26	4.77	2.07	2.77	23.58	2.06	5.40	3.29	2.98	4.06	1.56	1.88	1.61	3.49
Hf/Ta	4.39	27.79	0.21	4.35	4.04	12.29	5.54	9.18	12.04	14.06	9.14	15.08	11.16	7.00	7.26	10.93	9.11	8.05	14.03	8.34	9.13
Th/U	3.27	4.17	15.28	12.92	6.28	11.78	6.15	1.97	4.83	7.82	3.41	1.90	9.86	0.34	3.64	2.72	1.29	17.54	16.73	17.37	6.33
LaN/YbN	5.68	32.82	26.19	9.85	37.96	37.88	34.17	10.76	7.53	7.81	21.25	12.86	21.13	19.29	29.61	28.41	21.61	35.76	50.61	49.43	4.06
Eu/Eu*	0.92	1.14	1.02	0.52	0.41	0.61	0.72	0.86	0.92	0.93	0.66	0.68	0.82	0.50	0.65	0.71	0.56	0.81	0.84	0.64	0.84

between angular breccia parts. When first samples were studied in mid-2000, parts of the breccia zone were already strongly weathered. Upon a more recent visit in 2001, it was found that the entire core had been exposed to several months of hot weather and substantial rainfall, which had led to complete disintegration of the entire important breccia zone.

Quartz grains with PDFs do occur in the suevitic breccia, but not very abundantly. The estimated proportion amounts to <0.01 vol%. The crystallographic orientations of PDFs in a number of quartz grains were measured on the optical microscope and employing a 4-axis universal stage (Reinhard, 1931; Emmons, 1943). The results of these measurements are shown in Fig. 7 in the form of a plot of the frequency of indexed PDFs *vs.* angles between the *c*-axes of the host quartz grains and the poles to PDF planes. The data in this figure were obtained from stereographic projection of poles to PDFs after transformation of the optic axis into a vertical projection, following the method described, for example, by Engelhardt and Bertsch (1969). Usage of a standard stereographic projection of rational crystallographic planes in quartz showed that 42 of the 52 measured sets can be indexed. These 52 PDF measurements were observed in 33 grains: 18 grains contained 1 set; 11 contained 2 sets; and 4 contained 3 sets. The results of the orientation measurements clearly show that most of the shock-characteristic orientations are present with several dominant peaks (*e.g.*, for the $\{10\bar{1}3\}$, $\{10\bar{1}1\}$, $\{11\bar{2}1\}$ and $\{2\bar{1}\bar{3}1\}$ zones). These results, and other observations of shock metamorphic effects described above, confirm the Kgagodi Basin as a definite impact structure.

GEOCHEMISTRY

All of the major lithologies encountered in the core samples were analyzed for major and trace element composition. Major element analyses and abundances of selected trace elements were obtained on powdered samples by standard x-ray fluorescence (XRF) procedures (see Reimold *et al.*, 1994, for details). All other trace elements were analyzed by instrumental neutron activation analysis (INAA), following the procedures described by Koeberl (1993). The results of the analyzed samples of target rocks and breccias are summarized in Table 1. Table 2 provides detail regarding sample identification. Some breccias and fractured basement rocks are, as mentioned above, impregnated with secondary carbonate, which complicates chemical interpretation. These samples can be readily identified in Table 1 from the high loss-on-ignition (LOI) values that coincide with high CaO contents.

Most samples representing country rocks are of granitic or amphibolitic composition and are derived from the regional Archean basement. In addition, a Karoo gabbro (#43) and several breccia samples were analysed. Figure 8 illustrates the highly variable compositions of the different lithologies. It also shows an obvious trend for the granitoid/amphibolite samples towards the CaO corner of this diagram with increasing

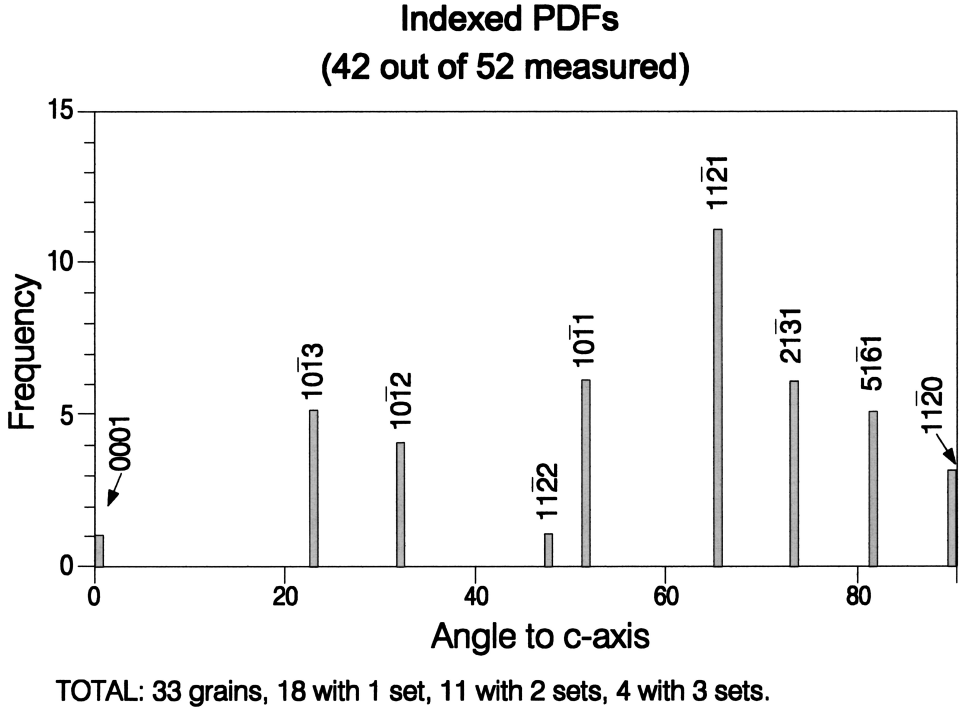

FIG. 7. Results of PDF measurements: frequency of indexed PDFs *vs.* angle between the *c*-axes of the quartz grains and the poles to the PDFs. $N = 52$ is the total number of measurements. Of these, 42 data could be unequivocally indexed with Miller indices.

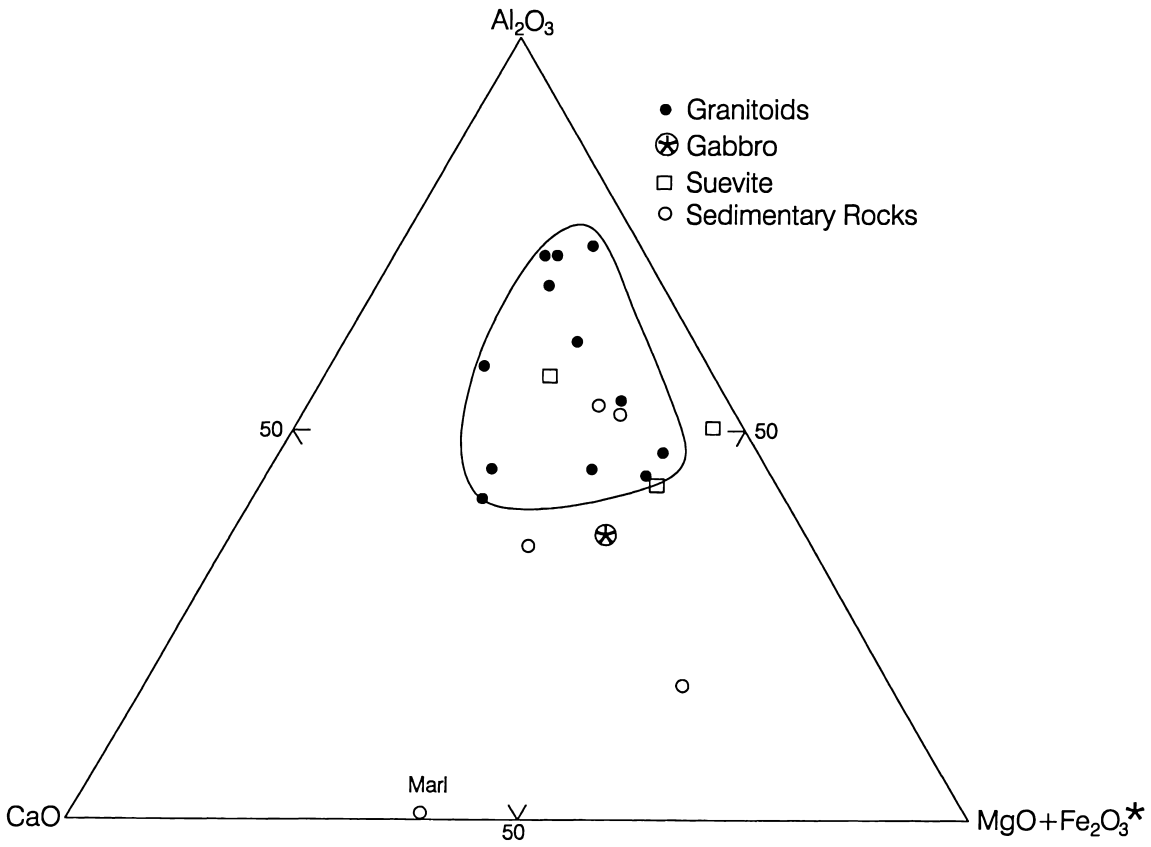

FIG. 8. Al_2O_3–CaO–MgO + Fe_2O_3 ternary plot, for major lithologies in the Kgagodi drill core. *Total Fe as Fe_2O_3. The field characterizing the variety of compositions of crystalline basement lithologies is emphasized by a thin line.

TABLE 2. Ir contents on selected samples using γ-γ coincidence spectrometry.

Sample no.	Rock type	Ir (ppt)
2	Schist	83 ± 13
2A	Granitoid	28 ± 10
3	Granitoid	50 ± 14
4A	Granitoid	68 ± 12
6A	Granitoid	65 ± 16
6B	Amphibolite	59 ± 15
7C	Suevitic breccia	48 ± 8
7E	Suevitic breccia	152 ± 20
7F	Suevitic breccia	119 ± 21
7G	Suevitic breccia	105 ± 15
7J	Granite gneiss	151 ± 24
7K	Suevitic breccia	248 ± 35
14E	Breccia (clast-dominated)	25 ± 10
41	Basement granitoid	41 ± 13
42	Granite	35 ± 12
43	Gabbro	38 ± 12
154m	Limestone	45 ± 13
158m	Granitoid breccia	76 ± 17
160.5m	Granitoid breccia	73 ± 17
161m	Granitoid breccia	98 ± 19
165m	Granitoid breccia	82 ± 18

contamination with secondary carbonate. This chemical variability is also seen in the abundances of trace elements, for example the rare earth elements (REE), patterns for which are shown in Fig. 9. With the exception of the gabbro sample #43 (data for which are also shown in Fig. 9) that displays a lesser degree of light (L)REE/heavy (H)REE fractionation, the other basement samples (clasts in impact breccia, in crater fill, or parautochthonous material from the crater floor) are characterised by relatively steeper patterns and more or less distinct negative Eu anomalies. The range of compositions is large and clearly dependent on the variable ratio of felsic to mafic minerals in this sample suite.

The suevitic breccias also have quite variable major element compositions, but with regard to REEs are much more homogeneous than the basement rocks. However, for many other trace elements (Table 1), significant heterogeneity is noted. Based on the petrographic observations, this can be explained by two main effects: different proportions of granitic, amphibolitic, and gabbroic clasts as well as variable degrees of impregnation with secondary carbonate (compare Fig. 8).

A comparison of abundances of elements that could possibly indicate the presence of a meteoritic component (*e.g.*, Co, Ni, Cr; Table 1) does not provide a straightforward picture. The

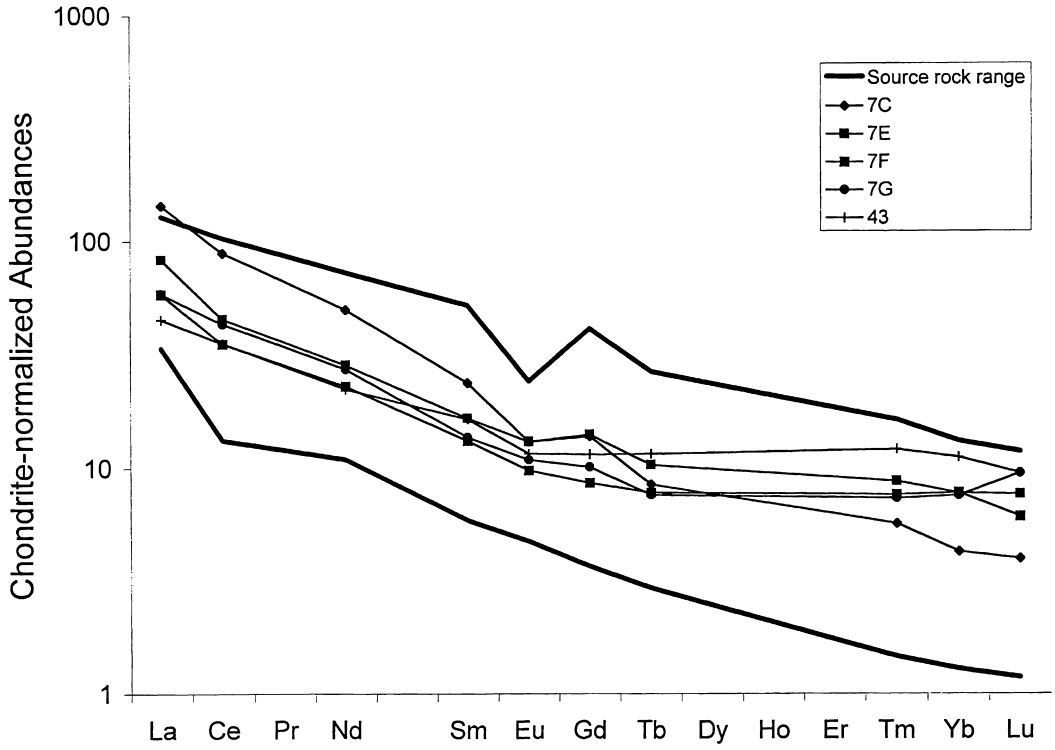

FIG. 9. Chondrite-normalized trace element abundances for selected samples (see Table 1 for rock types). C1 normalization factors after Taylor and McLennan (1985).

samples representing possible target rock components are characterised by widely different abundances of these elements, and ranges for basement rocks and suevitic breccias overlap (*e.g.*, Ni = 7–69 ppm in basement rocks and 25–66 ppm in suevitic breccias). However, including two suevitic breccias that are dominated by clastic material (from 157.8 and 157 m) increases the Ni values to 138 ppm for samples from this zone. Cobalt and Cr abundances are also quite high in the sample from 157 m depth (Co = 24.8 ppm and Cr = 476 ppm). Still, these results do not provide a clear indication whether the breccia zone may contain a meteoritic contribution. Therefore, selected basement and breccia samples were analysed for their Ir contents using γ-γ multiparameter coincidence spectrometry after neutron irradiation. This method allows the (instrumental) determination of Ir with detection limits of a few parts per trillion; for details of the instrumentation, measurements, standards, data reduction, precision, and accuracy, see Koeberl and Huber (2000). The results of the γ-γ coincidence spectrometry analysis for Ir in selected Kgagodi samples are listed in Table 2. They do not leave any doubt that several breccia samples have significantly higher Ir contents compared to the presumed target rock lithologies. Considering that the drill core only sampled the outermost part of the impact breccia lens within the Kgagodi structure, these data provide a good indication for the presence of a meteoritic component in Kgagodi suevitic breccia.

AGE CONSTRAINTS

No absolute dates have yet been obtained from any core samples, but certain age constraints may be applied based on the clast population observed in the suevitic breccia and a limited paleontological signature of the crater fill. The detection of apparent Karoo-age gabbro clasts in the breccia provides an upper age limit for the impact event at 180 Ma (*e.g.*, Hargraves *et al.*, 1997). Paleontological evidence includes various invertebrate microfossils and palynomorphs. The first (lowermost) occurrence of microfaunal remains occurs at 154 m, close to the base of the sedimentary crater-fill sequence. These remains have been identified as high spiraled gastropods (probably turritellids) and suggest an early Tertiary age based on comparison with marine forms (J. Smit, Vrije Universiteit Amsterdam, pers. comm., 2002). The rest of the sequence is dominated by ostracods and brachiopods that only offer very limited age control. A single layer at 55 m has proved productive for palynomorphs. However, once again their age is only loosely constrained. The palynomorph assemblage is dominated by reticulate spores (*Jania reticulates*) and *Podocarpites* sp., and also includes zooplankton and dinoflaggelate cysts. Most of the palynoflora represents long-range species that have a late Cretaceous to early Tertiary record. Therefore, based on the limited paleontological signature, the age of the fill of the crater can, so far, only be loosely estimated between late Cretaceous and early Tertiary

times, with the gastropod evidence near the base of the sequence favouring an early Tertiary age for the formation of the structure.

Although having no real bearing on the impact age problem, the enigmatic presence of *Acinosporites*, a Devonian-Carboniferous form, coupled to the different colors of the palynomorphs, in a sample from 56 m depth in the crater fill, suggests reworking of palynomorphs from older deposits. This is consistent with findings of Karoo age clasts in suevitic breccia, from which it can be inferred that the meteorite impacted into Carboniferous Dwyka group deposits.

Such a considerable age of this impact structure could also explain the earlier observation that the drainage pattern in the environs of Kgagodi does not seem to have been disturbed by the formation of the impact structure. Consistent with a considerable age is also the finding that the crater rim appears to be completely eroded, leaving an essentially flat topography over the crater structure.

On the basis of preliminary palynology results, the crater could well be of late Cretaceous to early Tertiary age. A more detailed account and interpretation of the palynology results will be given in a separate paper.

SUMMARY AND CONCLUSIONS

A 240 m long drill core was obtained <400 m inside of the rim of the ~3.5 km diameter Kgagodi Basin in eastern Bostswana. The rocks in the core comprise some 158 m of sedimentary rocks, followed by some 10 m of impact breccia, overlying granitic gneisses of the Limpopo Belt Central Zone. A gravity survey along two perpendicular traverses across the basin indicated a central negative Bouguer anomaly of 10 mGals. Modelling of these results suggested that the basin is filled with low-density sedimentary (brecciated) rocks to a depth of ~900 m and also confirmed the diameter of the basin to be 3 to 4 km. No evidence of a central gravity high was found from the gravity data. In addition, a magnetic survey was performed across the structure and showed a distinct difference in the magnetic signature, with a magnetically quiet section across the sedimentary infill and a more noisy signal outside of the basin limits.

Detailed logging of the core and petrographical and geochemical analysis on selected drill core samples were carried out. The results from these studies allow to divide the core into four zones: 0–158 m, basin fill; 158–165 m, suevite; 165–254 m, variably brecciated or fractured granitoids with melt breccia injection (240 m); and >254 m, undeformed granitic and minor amphibolitic basement. We also found melt and devitrified glass fragments in the suevite with abundant quartz and feldspar clasts containing multiple sets of PDFs. The major element data suggest that the suevite was mainly formed from granitoids, but also included significant mafic (gabbro) and small sedimentary components, which is in good agreement with the petrographic findings regarding clast population in the suevite breccia. Siderophile element enrichments were noted in the suevite compared to the target rocks. This is especially noticable from γ-γ coincidence spectrometry data for Ir, which are enriched in some suevite samples by a factor of up to ~5, compared to Ir abundances in target lithologies. Thus, the suevites most likely contain a minor, but significant, extraterrestrial component, equivalent to ~0.02% of a chondritic meteorite contribution. This is similar to values obtained for impact breccias from a number of other impact structures (cf., Koeberl, 1998).

Acknowledgments–We are grateful to Andrea Sanderson and Marion Bamford (Bernard Price Institute of Palaeontological Research, Wits University), and Jan Smit (Vrije Universiteit, Amsterdam) for their palynological support of this study. The Impact Cratering Research Group (ICRG) at the University of the Witwatersrand is funded through a grant from the University of the Witwatersrand Research Council. The geochemical work was supported by the Austrian Science Foundation, project Y58-GEO (to C. K.). We thank the Director of the Botswana Geological Survey Department for funding the drilling of the Kgagodi Basin. Critical reviews by David Kring and M. Yasunori resulted in improvement of the manuscript. This is Wits Impact Cratering Research Group Contribution No. 42.

Editorial handing: R. A. F. Grieve

REFERENCES

ENGELHARDT W. V. AND BERTSCH W. (1969) Shock induced planar deformation structures in quartz from the Ries crater, Germany. *Contrib. Mineral. Petrol.* **20**, 203–234.

EMMONS R. C. (1943) The universal stage (with five axes of rotation). *Geol. Soc. Am., Memoir* **8**, 1–205.

HARGRAVES R. B., REHACEK J. AND HOOPER P. R. (1997) Palaeomagnetism of the Karoo igneous rocks in Southern Africa. *South African J. Geology* **100**, 195–212.

KOEBERL C. (1993) Instrumental neutron activation analysis of geochemical and cosmochemical samples: A fast and proven method for small sample analysis. *J. Radioanal. Nucl. Chem.* **168**, 47–60.

KOEBERL C. (1994) African meteorite impact craters: Characteristics and geological importance. *J. African Earth Sci.* **18**, 263–295.

KOEBERL C. (1998) Identification of meteoritical components in impactites. In *Meteorites: Flux with Time and Impact Effects* (eds. M. M. Grady, R. Hutchinson, G. J. H. McCall and D. A. Rothery), pp. 133–152. Geological Society of London, Special Publication **140**, London, U.K.

KOEBERL C. AND HUBER H. (2000) Optimization of the multiparameter γ-γ coincidence spectrometry for the determination of iridium in geological materials. *J. Radioanalyt. Nucl. Chem.* **244**, 655–660.

MASTER S. AND REIMOLD W. U. (2000) The impact cratering record of Africa: An updated inventory of proven, probable, possible, and discredited impact structures on the African continent. In *Catastrophic Events and Mass Extinctions: Impacts and Beyond.* pp. 131–132. Lunar and Planetary Institute Contrib. **1053**, Lunar and Planetary Institute, Houston, Texas, USA.

MCCOURT S. AND VEARNCOMBE J. R. (1992) Shear zones of the Limpopo Belt and adjacent granitoid-greenstone terranes: Implications for late Archaean collision tectonics in southern Africa. *Precambrian Res.* **55**, 553–570.

PAYA B. K., HOLMES H., REIMOLD W. U. AND FARR J. (1999) Kgagodi Basin: A possible impact structure. *62nd Annual Meeting of the Meteoritical Society, Johannesburg,* late submission and poster.

REIMOLD W. U., KOEBERL C. AND BISHOP J. (1994) Roter Kamm impact crater, Namibia: Geochemistry of basement rocks and breccias. *Geochim. Cosmochim. Acta* **58**, 2689–2710.

REIMOLD W. U., PAYA B. K., HOLMES H., BRANDT D., KOEBERL C., DLADLA C. AND HANCOX P. J. (2000) Kgagodi Basin, Botswana: Origin by meteorite impact confirmed! (abstract). *Meteorit. Planet. Sci.* **35 (Suppl.)**, A135.

REINHARD M. (1931) *Universaldrehtischmethoden*. Birkhauser Verlag, Basel, Switzerland. 118 pp.

TAYLOR S. R. AND MCLENNAN S. M. (1985) *The Continental Crust: Its Composition and Evolution.* Blackwell Scientific Publications, Oxford, U.K. 312 pp.

THOMAS C. M. (1971) The geology of Selibe area. In *Geol. Surv. Botswana, Internal Report*. Geological Survey of Botswana, Lobatse, Botswana. 22 pp.

THOMAS D. S. G. AND SHAW P. A. (1990) The deposition and development of the Kalahari group sediments, central southern Africa. *J. African Earth Sci.* **10**, 187–197.

WATKEYS M. K. (1983) Brief explanation notes of the provisional geological map of the Limpopo Belt and environs. In *The Limpopo Belt* (eds. W. J. Van Biljon and J. H. Legg), pp. 5–8. Geol. Soc. S. Afri. Spec. Publ. **8**, Johannesburg, South Africa.